Ammonia Mobility in Chabazite: Insight into the Diffusion Component of the NH_3-SCR Process

Alexander J. O'Malley,[ab] Iain Hitchcock,[d] Misbah Sarwar,[d] Ian P. Silverwood,[c] Sheena Hindocha,[d] C. Richard. A. Catlow,[ab] Andrew P. E. York [d] and P. J. Collier[b,d*]

[a] *University College London, Department of Chemistry, Materials Chemistry, Third Floor, Kathleen Lonsdale Building, Gower Street, London WC1E 6BT, UK. E-mail: a.o'malley@ucl.ac.uk*

[b] *UK Catalysis Hub, Research Complex at Harwell, Rutherford Appleton Laboratory, Harwell Oxford, Didcot, Oxfordshire OX11 0FA, UK*

[c] *ISIS Facility, STFC Rutherford Appleton Laboratory, Didcot, Oxon OX11 0QX, UK.*

[d] *Johnson Matthey Technology Centre, Blounts Court, Sonning Common, Reading RG4 9NH, UK. Email: paul.collier@matthey.com*

Abstract

The diffusion of ammonia in commercial NH_3-SCR catalyst Cu-CHA was measured and compared with H-CHA using quasielastic neutron scattering (QENS) and molecular dynamics (MD) simulations to assess the effect of counterion presence on NH_3 mobility in automotive emission control relevant zeolite catalysts. QENS experiments observed jump diffusion with a jump distance of 3 Å, giving similar self-diffusion coefficient measurements for both C- and H-CHA samples, in the range of ca. 5-10 x 10^{-10} m^2s^{-1} over the measured temperature range. Self-diffusivities calculated by MD were within a factor of 6 of those measured experimentally at each temperature. The activation energies of diffusion were also similar for both studied systems: 3.7 and 4.4 kJ mol^{-1} for the H- and Cu- chabazite respectively, suggesting that counterion presence has little impact on ammonia diffusivity on the timescale of the QENS experiment. An explanation is given by the MD simulations, which showed the strong coordination of NH_3 with Cu^{2+} counterions in the centre of the chabazite cage, shielding other molecules from interaction with the ion, and allowing for intercage diffusion through the 8-ring windows (consistent with the experimentally observed jump length) to carry on unhindered.

1. Introduction

The need to minimise the air pollution caused by NO_x gases emitted from internal combustion engines has lead to the development of a number of technologies associated with lean-NO_x reduction. Catalytic solutions are particularly desirable for economic and efficiency reasons[1] , and a recently commercialised process under intensive research is the selective catalytic reduction (SCR) of NO_x to N_2 using ammonia with metal exchanged zeolite catalysts.[2, 3]

Despite the promising activity of Cu- and Fe- zeolite beta[4-8], practical concerns arose from both a durability perspective, and the poisoning of these medium pore width zeolites due to strongly adsorbing hydrocarbons from uncombusted fuel.[9] Research was then directed towards the smaller pore zeolites based on the chabazite (CHA) structure[10-13] with Cu-CHA zeolites now commercialised for NH_3-SCR catalysis in vehicle emission control, following studies showing their improved performance over metal doped beta and ZSM-5 catalysts.[14]

For development and optimisation of such catalysts, not only must the intrinsic NH_3-NO reaction kinetics and active site chemistry be understood, but also the diffusion processes limiting the molecular transport. Indeed, properties such as the effective diffusivity (D_e) are key descriptors in heterogeneous catalysis, used for the improvement and understanding of properties such as observed catalyst activity under diffusion limited conditions. There are several experimental methods, both microscopic and macroscopic which exist for obtaining diffusion coefficients, which however, can provide values which may differ by several orders of magnitude.[15] A detailed discussion of the different methods of measuring diffusivity in microporous solids can be found by Kärger,[16] where a detailed account of the theory underpinning different diffusivity measurements and information on microscopic and macroscopic methods is given. Such an understanding of diffusion behaviour is especially important for smaller pore zeolite structures where the kinetic diameters of the sorbates approach those of the channels. Intracrystalline diffusion limitations, which complicate traditional kinetic studies[17] in Cu-CHA NH_3-SCR have been investigated by Gao et al[18] who concluded significant mass-transfer limitations on the reaction rate with increasing Cu^{2+} content. It has also been shown in model catalyst samples at relatively low temperatures on a per Cu atom basis, that Cu-ZSM-5 and Cu-Beta exhibited higher activities than Cu-CHA,

potentially due to such mass transfer limitations.[19] The behaviour and mobility of the counterion (the catalytic centre) is of course crucial to determining structure-activity relationships. At low loadings the Cu^{2+} is located within the 6-rings[20, 21] however upon adsorption and interaction with gases the ion is then pulled into the chabazite cages with an increase in mobility. [22]

Despite its relevance to the NH_3-SCR process, very few direct studies of ammonia diffusion in zeolites have been reported. A problem faced by macroscopic measurements is that the heat of adsorption for ammonia in zeolites is large. Therefore, uptake measurements will generally be dominated by phenomena other than intracrystalline diffusion, often intercrystalline diffusion within the bed, or the effects of local heating.[23] Microscopic methods, which focus on molecular motion, are able to sample this intracrystalline diffusion at equilibrium. Ammonia diffusivity in silicalite has been studied using the microscopic measurement techniques of quasielastic neutron scattering (QENS) and pulsed field gradient NMR (PFG-NMR).[24] An advantage of the differing timescales sampled by the two techniques is illustrated as the longer timescale (μs) accessed by PFG-NMR detected both trapped and diffusing molecules, leading to an average diffusivity lower than that measured by QENS (sampling timescales of motion on the nanoscale). Upon investigating the effect of loading on NH_3 diffusion, it was found that the diffusivities increased with loading, suggesting trapping upon interaction with silanol defects. Other PFG-NMR studies have also examined ammonia diffusion in ZSM-5, agreeing with the observation of increased diffusivity with loading due to the progressive saturation of adsorption sites.[25, 26] On a macroscopic scale, TPD studies have been used to decouple quantitative information on mass transfer and adsorption properties in H-ZSM-5,[27] and measure diffusivity significantly higher in H-ZSM-5 than NaY.[28]

The insight gained from these microscopic techniques illustrates the potential for detailed study of the diffusion component of the NH_3-SCR process. In particular, microscopic experimental diffusion studies in zeolites are greatly aided by their pairing with molecular dynamics (MD) simulations. The complementarity of QENS and MD in studying sorbate diffusion in zeolites has been previously discussed [29], and illustrated by recent studies using state-of-the-art models for the framework and sorbate in simulating the self-diffusion of longer n-alkanes[30, 31] and isobutane[32] in silicalite. The close agreement in measured

theoretical and experimental self-diffusion coefficients (D_s), and potential qualitative and quantitative insight into dynamical behaviour on the nanoscale observable though this combination of methods make for a particularly suitable approach for the study of ammonia diffusion in CHA zeolites. The role of the counterion may also be assessed through direct comparison of ammonia self-diffusivity in samples with and without the Cu^{2+} counterion present. Indeed, the effect of counterion presence was studied by Jobic in MFI zeolites using QENS, comparing the diffusivities of longer *n*-alkanes in silicalite[33] and Na-ZSM-5[34], measuring faster mobility in the former by a factor of 3.8-5.2 depending on chain length.

In this study, we combine QENS experiments with MD simulations to measure the diffusion of ammonia in the commercially used Cu-CHA, in comparison with H-CHA. We find good agreement in measured D_s between the two methods, and an unexpected comparison between the two zeolite samples, where the coordination of ammonia to the Cu^{2+} ion plays a significant role in the observed behaviour.

2. Experimental

The materials studied in this work were a commercially available H-CHA zeolite and 3 wt.% Cu-CHA zeolite. Both samples were in powder form and microporous only as determined by nitrogen gas adsorption at 77 K.

2.1 Quasielastic Neutron Scattering Experiments

A detailed discussion the QENS method and its applicability to deriving dynamical characteristics of sorbates in zeolites can be found in reference 29.

All measurements were performed using time-of-flight backscattering neutron spectrometer OSIRIS [35] at the ISIS Pulsed Neutron and Muon Source, Rutherford Appleton Laboratory, Oxfordshire. Pyrolytic Graphite 002 analyser crystals were used to give an energy resolution of 24.5 μeV with energy transfers measured in a window of ±0.55 meV.

The CHA and Cu-CHA samples were placed in stainless steel can and heated to 300°C overnight at vacuum to remove any pre-adsorbed water. After cooling, the can was

transferred to a glovebox under an argon atmosphere. The dry sample (3.1 grams in total) was transferred to a thin walled aluminium container of annular geometry. The aluminium cell was then connected to a gas inlet system, which allowed ammonia to be adsorbed onto the zeolite. The cell pressure was raised to 800 mbar to ensure the zeolite was saturated with ammonia. In this study we have not considered partial NH_3 loadings; although an understanding of the preferred location of NH_3 molecules as a function of loading is an important consideration for future study it is outside the scope of this work. The QENS experiments were performed at 273, 323 and 373 K. In addition, the scattering of the dehydrated zeolite was recorded at each temperature and subtracted from the spectra recorded with adsorbed ammonia. The elastic resolution function was measured with a vanadium sample. All data were analysed using a combination of Mantid[36] and DAVE softwares.[37]

2.2 Molecular Dynamics Simulations

Molecular Dynamics simulations were run using Forcite as implemented in Materials Studio 8.0 [38]. The simulations were run at 273K, 323K and 373K to provide direct comparison with QENS measurements. The coordinates of the CHA structure were obtained from the IZA database.[39] A 2x2x2 supercell was created and periodic boundary conditions were used. The Si atoms in the 8-rings were randomly substituted with Al atoms to give a Si/Al ratio of 17, closely matching those of the experimental samples (previous work has shown that the energy difference between different Al configurations is relatively small[40]). Charge compensation was made by either Brønsted acid sites on O atoms adjacent to the Al or via Cu^{2+} ions placed in the channel centres. The Cu^{2+} ions were placed in the 8-ring only, as when they were placed in both the 6-ring and 8-ring, they were found to move out of the 6-ring windows into the cavity towards the 8-ring after NH_3 adsorption. Such movement of the ion on interaction with adsorbates has also been previously observed.[41]

Before the simulation, the NH_3 molecules and framework structures were optimised using the COMPASS forcefield [42] which was used to represent the intra and intermolecular forces throughout. Charges used are detailed in table 1. Standard forcefield charges were used for the H-CHA structure and NH_3 molecules. For the Cu-CHA structure the charges are applied according to Arl et al.[43]

The initial loading of the molecules was obtained by conducting a Monte Carlo Simulation as implemented in the Sorption Module in Materials Studio.[38] A fixed pressure simulation was run at 1 atm and 298 K to obtain an estimate of the experimental loading used for the QENS measurements which corresponded to a loading of 90 molecules per cell. These structures were then re-optimised and subjected to a simulated annealing procedure to ensure a low energy starting structure. As mentioned, periodic boundary conditions were used throughout and the non-bonded interactions were calculated by Ewald summation with a 12 Å cut-off. The zeolite framework was fully flexible in the simulations. The system was then equilibrated for 200 ps using a 1 fs time step, after which no statistically meaningful variation in energy was observed. Production runs were then started from these equilibrated systems and run for 1 ns, again using a timestep of 1 fs. The NVT ensemble, with a Nosé thermostat, was used throughout. The trajectory of the N atom was recorded every 250 steps during the course of the simulation. To understand the confinement effect of the zeolite framework on the diffusion of NH_3, an MD simulation for the same loading of NH_3 in the same sized cell as the CHA simulations without the framework present was also run. We refer to the NH_3 molecules in this case as "unconfined" NH_3. The calculations were run on a Dell Optiplex 7010 parallelised over 4 processors at Johnson Matthey Technology Centre.

Atom	q (esu)
H-CHA:	
Si	+0.890
Al	+0.7343
O	-0.445
O-Al	-0.4578
H	+0.0839
Cu-CHA:	
Si	+0.890
O	-0.445
O-Al	-0.620
Al	+0.590
Cu^{2+}	+2.000
Ammonia:	
N	-1.0590
H_a	+0.353

Table 1. Charges used for each element in the molecular dynamics simulation. O-Al denotes an oxygen atom bonded to an aluminium atom.

The mean squared displacements (MSD) obtained were evaluated for each temperature via the following equation:

$$\mathrm{MSD}(t) = \langle \Delta \mathbf{r}_j^2(t) \rangle = \frac{1}{N} \sum_{j=1}^{N} \Delta \mathbf{r}_j^2(t) = \frac{1}{N} \sum_{j=1}^{N} \left[\mathbf{r}_j(t) - \mathbf{r}_j(0) \right]^2 \quad (1)$$

where N corresponds to the number of NH_3 molecules and $\mathbf{r}_j(0)$ and $\mathbf{r}_j(t)$ to the initial and final positions of the molecular centre of mass over time interval t.

The diffusion coefficients were obtained by fitting the MSD against time in the region 0-500ps (where the profiles had a slope of 1.0), according to the Einstein equation:

$$MSD(t) = A + 6Dt \quad (2)$$

activation energies for self-diffusion were then obtained from an Arrhenius plot according to the Arrhenius equation:

$$D_s = e^{\left(\frac{-E_a}{RT}\right)} \quad (3)$$

3. Results and Discussion

3.1 Quasielastic Neutron Scattering Experiments

The QENS spectra at 323 K (50 °C) are shown in figures 1 and 2. We note that the spectra were fitted with the instrumental resolution function, a flat background and a single Lorentzian function suggesting one observable mode of motion on the instrumental timescale.

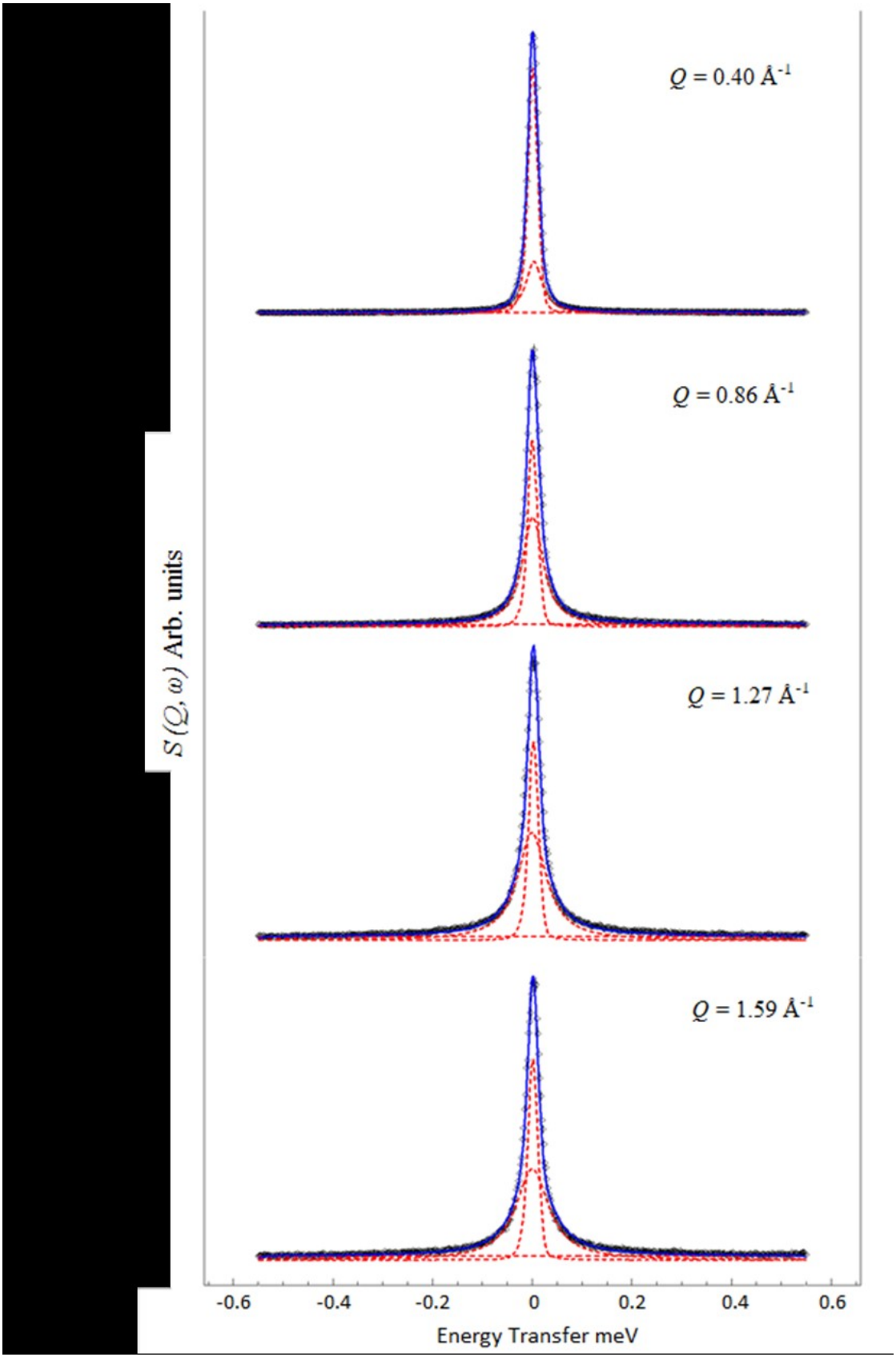

Figure 1. QENS spectra obtained for ammonia diffusing in H-CHA at 4 different Q values at 323 K. (**--**) is the total fit, and (**--**) are the constituent resolution, Lorentzian and flat background functions.

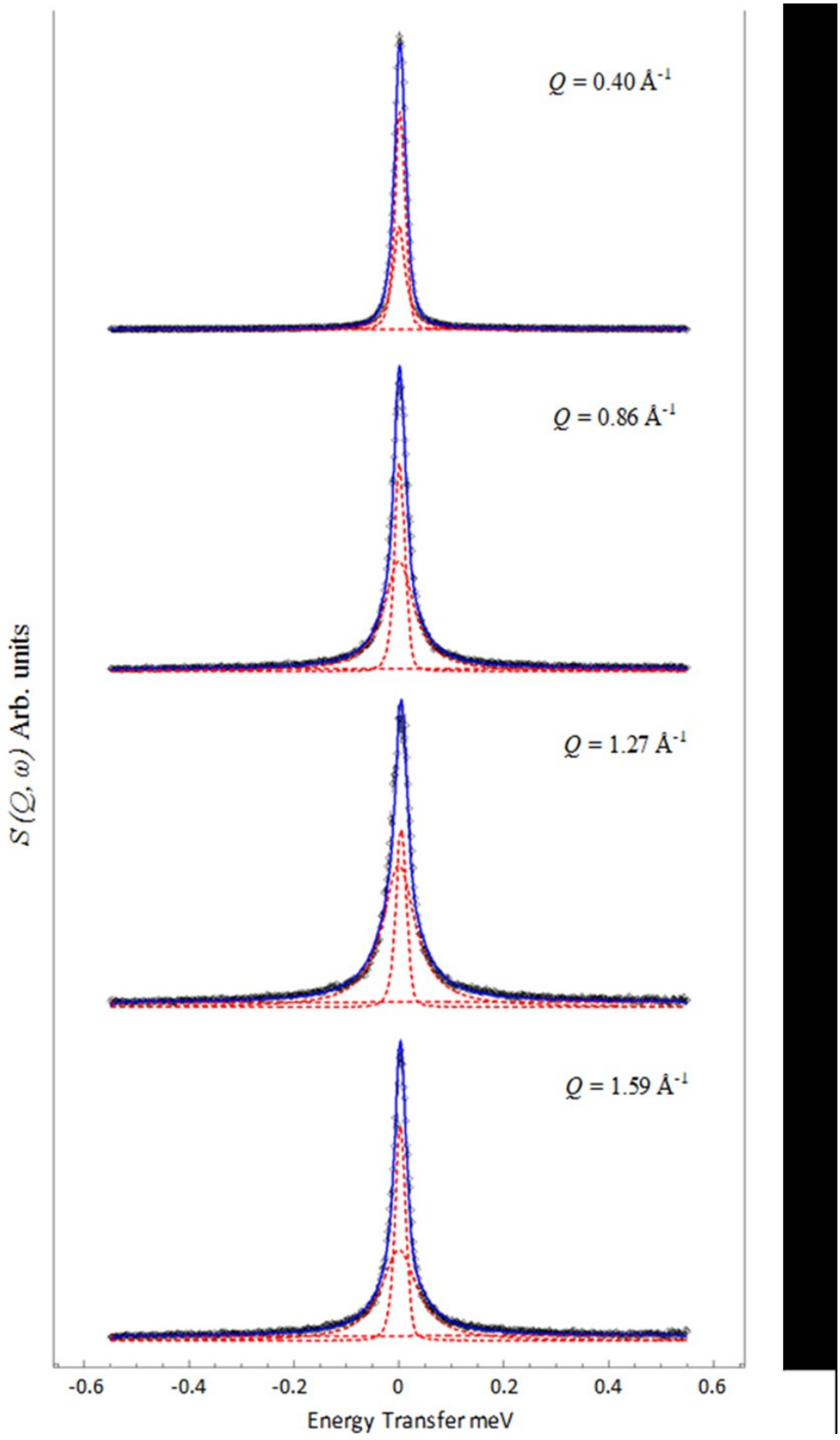

Figure 2. QENS spectra obtained for ammonia diffusing in Cu-CHA at 4 different Q values at 323 K. (--) is the total fit, and (--) are the constituent resolution, Lorentzian and flat background functions.

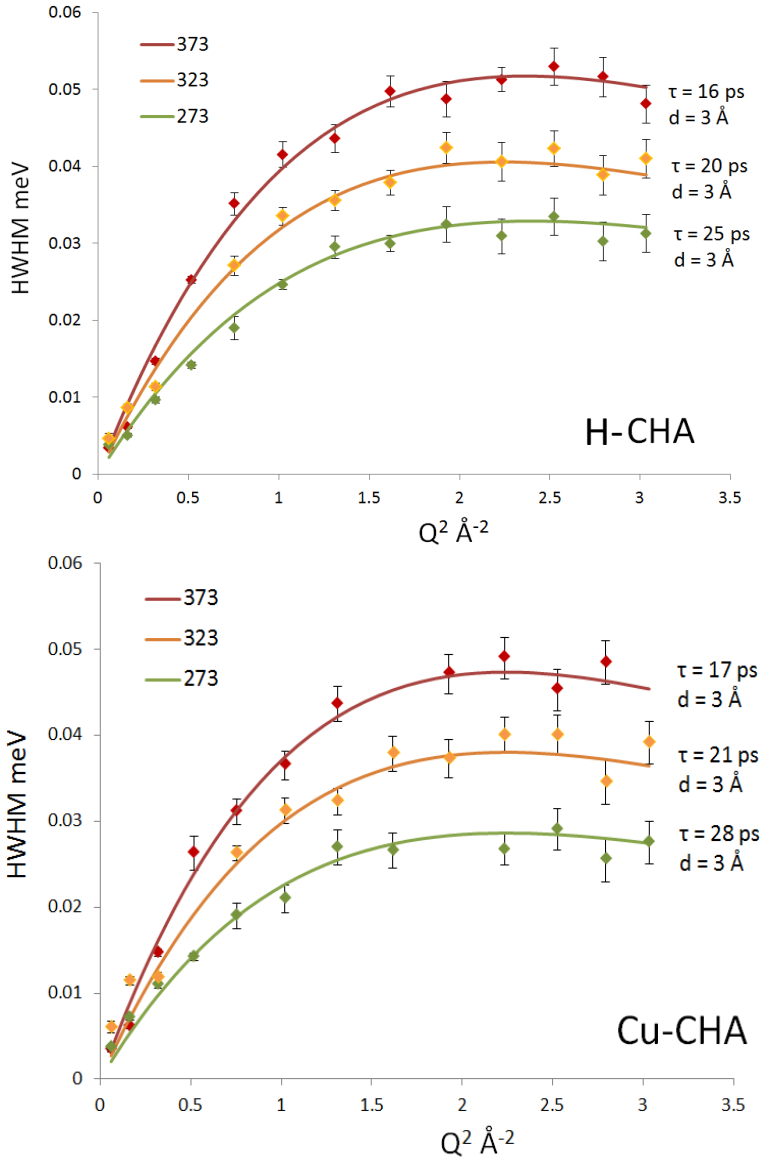

Figure 3. Q dependencies of the HWHM of the quasielastic components of the QENS spectra. Each can be fit with a jump diffusion model, jump parameters listed in each plot.

We observed (as shown in figure 3) that at all temperatures, for both systems, the ammonia fits approximately to the Chudley and Elliot jump diffusion model,[44] with a fixed jump length of 3 Å. We note that this length may correspond to either intracage jump diffusion or jump diffusion between cages in the chabazite structure. Jump residence times decrease over the 273 K to 373 K range from 25-16 ps in the H-CHA system and 28-17 ps in the Cu-CHA system. The self-diffusion coefficients were extrapolated as explained in reference 29, and are listed in Table 2. We note that the differences in diffusion coefficients at each temperature between systems are within experimental error despite being consistently higher for the bare H-CHA. The diffusion coefficients obtained are lower by a factor of 3 than those of ammonia obtained in silicalite in reference 24 (with a pore diameter ca. 1.5 Å wider than chabazite), though we note that our loadings are significantly higher than even the highest

loading in that study (4.3 mol/uc). As mentioned in section 2.1, our zeolite was fully saturated with ammonia and the dependence of ammonia loading on diffusivity will be addressed in a future study.

An important point to consider is the effect of crystallite size on the measured diffusivity of NH_3, which (depending on the method used to measure the diffusivity) may potentially be affected by surface barrier effects if the crystallite is too small as recently discussed by Dauenhauer et al.[45] This effect is not significant in our experiment, as the maximum length scale of movement detectable during the QENS experiment is on the order of ~20 nm, significantly less than the size of the zeolite crystals in our study (~1-2 µm). Therefore, our results will not be affected by surface barrier effects.

T K	273	323	373	Ea kJ mol^{-1}
H-CHA	6.0 x 10^{-10} ± 1.2 x 10^{-10}	7.6 x 10^{-10} ± 1.5 x 10^{-10}	9.4 x 10^{-10} ± 1.7 x 10^{-10}	3.7
Cu-CHA	5.4 x 10^{-10} ± 1 x 10^{-10}	7.1 x 10^{-10} ± 1..3 x 10^{-10}	8.8 x 10^{-10} ± 1.6 x 10^{-10}	4.4

Table 2. Values of D_s obtained using QENS of ammonia in both zeolites, in units of m^2s^{-1}.

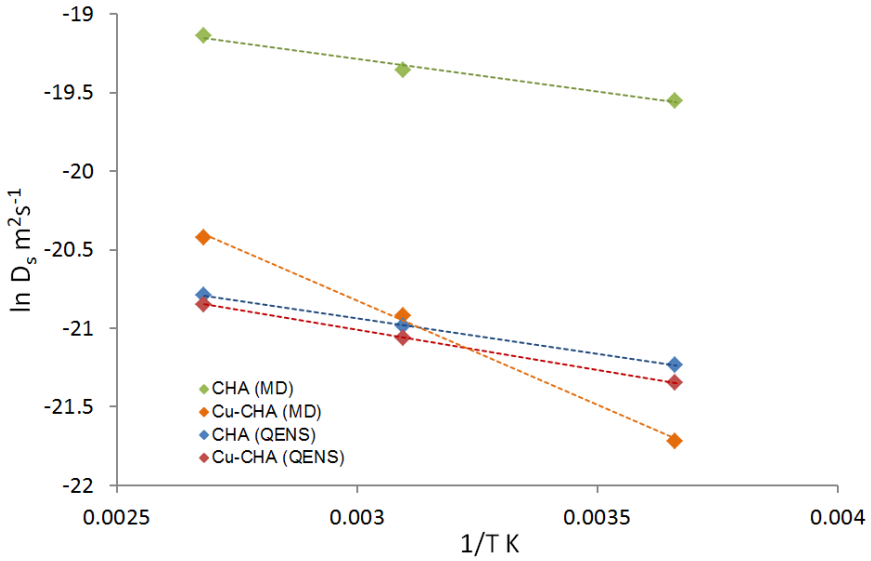

Figure 4. Arrhenius plots of ammonia diffusion in chabazite, giving activation energies of 3.7 and 4.4 kJ mol^{-1} in CHA and Cu-CHA respectively.

The activation energies are calculated using the Arrhenius plot in Figure 4. We obtain values of 3.7 kJ mol^{-1} for CHA and 4.4 kJ mol^{-1} for Cu-CHA. We note that these are 3.5 kJ mol^{-1} lower

than those obtained for ammonia in silicalite (though the authors note that the error on their measured diffusion coefficients obtained may be as high as a factor of 2). When considering the measured activation energies, we note that these are measured at saturation and there will be a difference in activation energy at different loadings. However, as mentioned previously the dependence of the measured diffusion coefficients on NH_3 loading is outside the scope of this work will be addressed in future studies.

3.2 Molecular Dynamics Simulations

Mean Squared Displacement (MSD) plots are presented in figure 5 for H-CHA and Cu-CHA at 273K, 323K and 373 K. They appear linear at all temperatures, indicating that the statistics in our simulations are sufficient for calculating accurate diffusion coefficients. The diffusion coefficients of NH_3 in H-CHA and Cu-CHA, along with unconfined gas phase NH_3 calculated from these plots are listed in table 3.

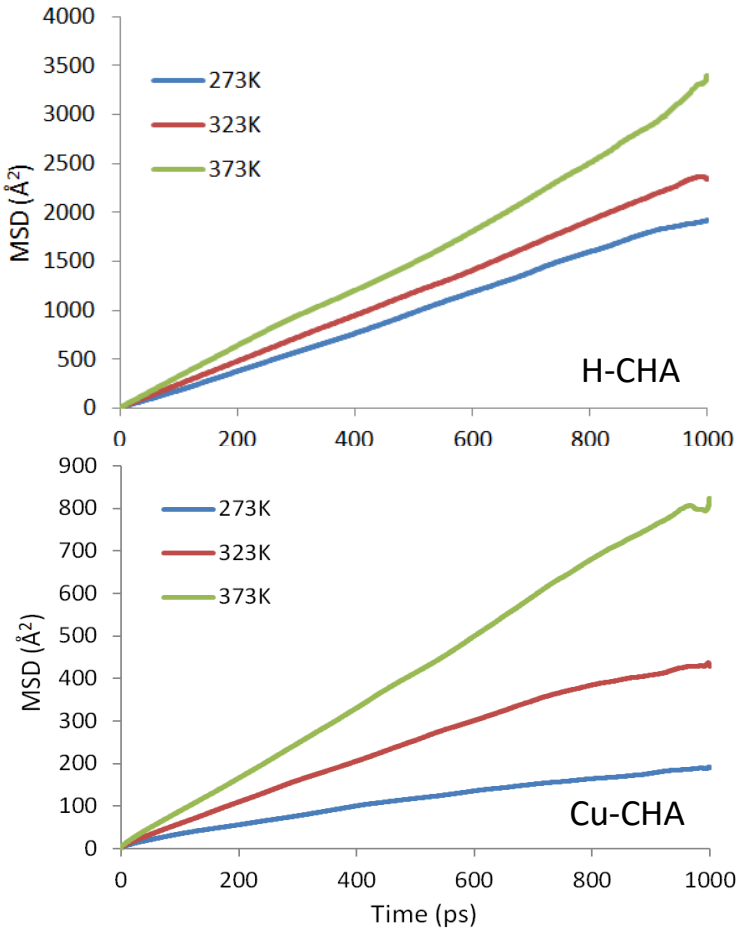

Figure 5: MSD plots for NH_3 in CHA (top) and Cu-CHA (bottom) at three different temperatures

The calculated diffusion coefficients are much lower in magnitude than those calculated for unconfined NH_3 using the same loading and temperature, indicating as expected that the confinement effect of the zeolite framework strongly affects the self-diffusivity of NH_3. The diffusion coefficients of NH_3 in Cu-CHA are lower than in H-CHA by a factor of 9, 4.5 and 4 at 273, 323 and 373 K respectively indicating that the self-diffusion of NH_3 is significantly affected by the presence of the Cu^{2+} counterion. The difference is in contrast to the QENS experiments where the measured D_s values are very similar. The activation energy of NH_3 diffusion in H-CHA (3.5 kJ mol^{-1}) is in good agreement with the QENS studies, however the large activation energy of 10.8 kJ mol^{-1} for Cu-CHA is also in contrast to that obtained from the QENS study, suggesting that in the simulation, the Cu^{2+} is a significant barrier to mobility. We note that the agreement in absolute D_s values between QENS and MD for the H-CHA system is roughly a factor of 5 as listed in table 5, reasonable and consistent with other studies employing state-of-the-art MD simulations employing a flexible zeolite framework for similar systems.[30-32] The agreement is considerably closer for the Cu-CHA system, however the significant discrepancy in activation energy and the much larger difference in simulated diffusivity between the two frameworks compared to experiment means this agreement must be treated with caution.

T (K)	**Unconfined NH_3 D_s (m^2s^{-1})**	**CHA D_s (m^2s^{-1})**	**CHA D_s(MD)/Ds(QENS)**	**Cu-CHA D_s (m^2s^{-1})**	**Cu-CHA D_s(MD)/D_s(QENS)**
273	$7.39x10^{-7}$	$3.23x10^{-9}$	5.40	$3.69x10^{-10}$	0.68
323	$1.43x10^{-6}$	$3.92x10^{-9}$	5.15	$8.22x10^{-10}$	1.15
373	$2.39x10^{-6}$	$4.90x10^{-9}$	5.21	$1.35x10^{-9}$	1.53
Ea kJ mol^{-1}		**3.5**		**10.8**	

Table 3. Diffusion coefficients for 90 NH_3 molecules in CHA at three different temperatures along with bulk NH_3.

A trajectory plot of the centre of mass of NH_3 in Cu-CHA at 323K is shown in figure 6. The plot shows that diffusion of NH_3 takes place exclusively via the 8-ring windows, which can be explained by comparing the size of the NH_3 molecule (2.6 Å) with the 6-ring and 8-ring windows in the CHA structure (2.7 and 3.8 Å respectively), thus the NH_3 molecule is sterically hindered and unable to pass easily through the 6-ring and diffusion occurs via the

8-rings. Our observation suggests that in the QENS experiments, the observed 3 Å jump diffusion is that of intercage diffusion through the 8-ring windows.

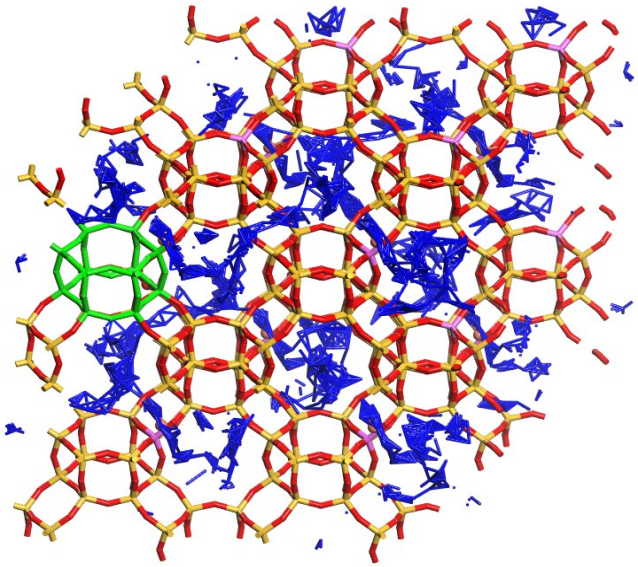

Figure 6. Trajectory plot of the centre of mass of NH_3 in Cu-CHA at 323K, showing no movement through the 6-ring windows (highlighted green). Frames were plotted every 250 ps over the entire trajectory.

An insight into the contrast in observed impact of counterion presence on NH_3 mobility between the QENS and MD method can be found upon examining the configurations of the MD simulation in the Cu-CHA system. A snapshot of the trajectory in figure 7 shows that NH_3 molecules tend to cluster around the Cu^{2+} ions with either 3 or 4 NH_3 molecules surrounding each Cu^{2+} ion, where the NH_3 molecules interact with each other and the zeolite framework via an extended hydrogen bonding network.

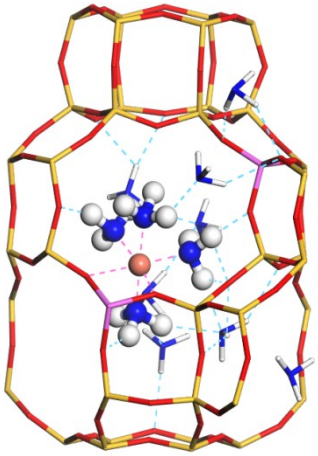

Figure 7. Cluster of NH_3 molecules surrounding Cu^{2+}. The blue dashed lines represent hydrogen bonds.

This clustering of the ammonia in the presence of Cu^{2+} is evident upon calculation of the radial distribution function (RDF) as shown in figure 8(a). For the Cu^{2+} counter ion and ammonia interactions, we observe a very intense peak at 2.05 Å for the Cu^{2+}--N distance, indicating a strong interaction between the Cu^{2+} ion and surrounding NH_3 molecules. When comparing the RDF plot of N--N(NH_3) distances between CHA and Cu-CHA in figure 8(b), the sharp peaks in the latter show the average N (from NH_3) is around 2.93 Å from each other at 273 K, the radius of the second sphere is at 4.1 Å and the third at 5.9 Å, which is indicative of stable NH_3 clusters. These clusters are not observed in H-CHA, where a broad peak in the RDF is observed at 3.93 Å, similar to previously calculated RDFs of liquid ammonia.[46]

We observe perturbation of these clusters at higher temperatures as shown in figure 8(c), where the intensities of the three peaks corresponding to the ammonia shells decrease suggesting a more disordered system. The effect of this clustering on the overall mobility of ammonia in the Cu-CHA system is considered by decoupling the MSD plots between coordinated and uncoordinated molecules, as shown in figure 9. These show especially at 273 K, that the NH_3 molecules that are coordinated to the Cu^{2+} ions show little or no diffusion indicating that they are quite stable and remain bound to the Cu^{2+} ion throughout the simulation (certainly immobile with respect to the timescale of the QENS experiment). However, the uncoordinated NH_3 molecules are able to diffuse freely.

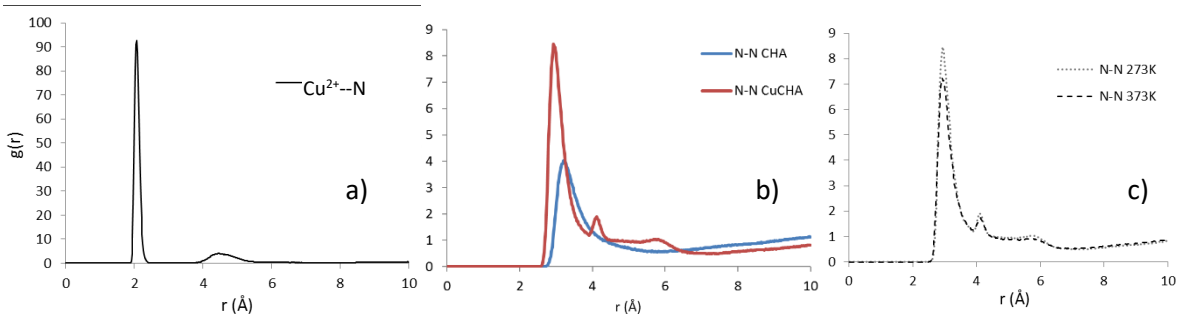

Figure 8. RDF plots of a) the Cu^{2+}--N (NH_3) distance in the Cu-CHA system, b) the N--N (NH_3) distances compared in the CHA and Cu-CHA systems, c) the N--N distances at 273 K and 373 K in the Cu-CHA system.

The diffusion coefficients obtained for the decoupled, uncoordinated NH_3 are faster than the total diffusion coefficients, and are listed in table 4, and also plotted in comparison with the experimental values and self-diffusivities of CHA in figure 10.

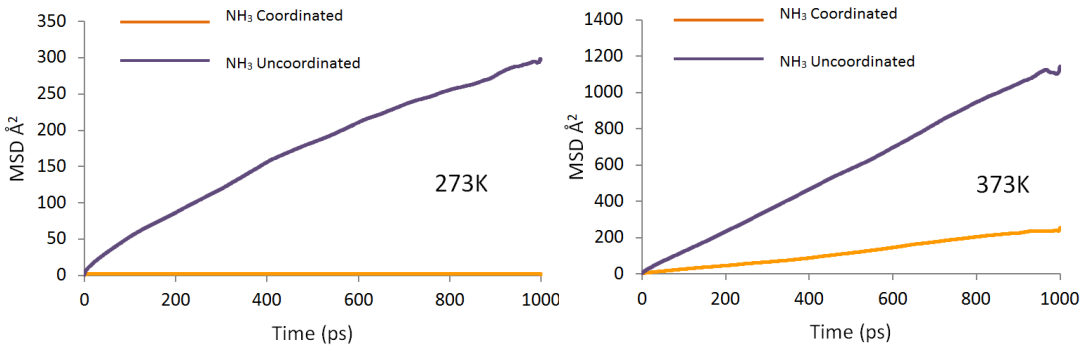

Figure 9. MSD plots at 273 K and 373 K for NH_3 molecules coordinated to the copper counterion and those not coordinated, illustrating the immobilising effect of counterion coordination on ammonia.

T K	Cu-CHA $D_{s\ (Uncoordinated)}$ m^2s^{-1}	Cu-CHA $D_{s\ (Uncoordinated)}$/ Ds (QENS)
273	5.76×10^{-10}	1.07
323	1.14×10^{-9}	1.39
373	1.9×10^{-9}	2.16

Table 4: Diffusion coefficients obtained from the MD simulations of the freely diffusing NH_3 molecules (decoupled from the Cu coordinated NH_3) in the Cu-CHA system and compared with experimentally measured values.

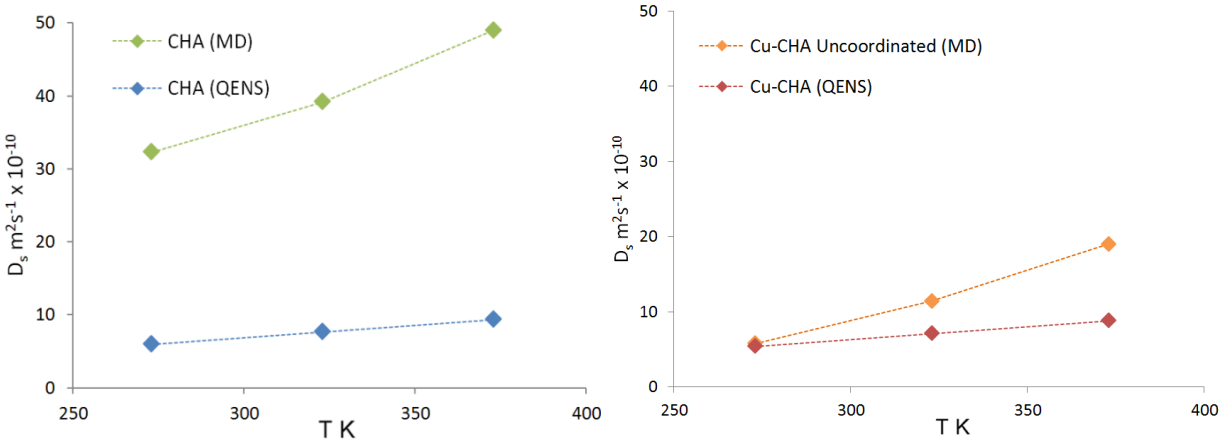

Figure 10. Diffusion coefficients plotted for comparison between QENS experiments and MD simulations in (left) the CHA system and (right) the Cu-CHA system.

We note that for both the H-CHA and Cu-CHA (when sampling the movement of the uncoordinated molecules) systems the diffusion coefficients are consistently higher for the MD simulations than the QENS measurements. This observation is common in microscopic studies of sorbate diffusion in zeolites, often attributed to the ideal zeolite crystal used in the simulation model. The experimental sample is likely to have defects, such as silanol nests, extra-framework aluminium and grain boundaries on the nanoscales which will lower

the diffusion coefficient. We also make the assumption in the Cu-CHA system of very evenly distributed Cu^{2+} counterions, where experimentally the dispersion of copper in zeolites can depend heavily on the preparation method and subsequent treatment as shown by previous XPS/XAES studies.[47] An additional reason for the observed difference may be the choice of force field used in our MD simulations. The COMPASS force field is a generic force field not developed and fitted for these specific systems. Despite the agreement achieved in this study it is important to recognise that in any generic force field there will be inherent approximations which can only be properly addressed through detailed empirical (or quantum mechanical) fitting of guest-host interactions.

Despite the good agreement which our revised analysis gives of diffusion coefficients between the MD and QENS studies, the activation energy for the uncoordinated NH_3 molecules is calculated to be 10.1 kJ mol^{-1}. We note that this is still 5.7 kJ mol^{-1} higher the experimental value. Although we must also consider the inherent approximations of the generic force field in our calculation, an important consideration is that the QENS technique is limited by the resolution of the instrument, which is not sensitive to movements taking place over timescales longer than 200 ps. Examination of the MSD plot for a single ammonia molecule in Cu-CHA at 323 K, depicted in figure 13 shows a range of residence times (indicated by a plateauing of the MSD) on the order of ~5 ps and up to residence times close to the limit of the instrument.

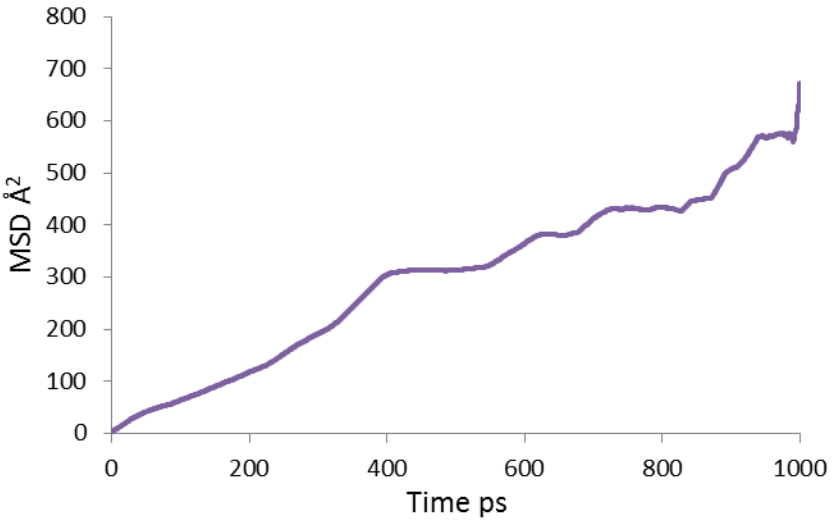

Figure 11. The MSD plot of an individual NH_3 molecule in the Cu-CHA system at 323 K, exhibiting jump diffusion behaviour of differing residence times, some of which approach the resolution limit of the OSIRIS spectrometer.

This limit means that certainly those molecules coordinated to Cu^{2+} which remain stationary for the total 1 ns simulation will not move over a timescale sensitive to our instrument. Measuring the movement of these molecules would necessitate higher resolution methods such as the neutron spin echo technique, which are able to sample jump diffusion with residence times on the order of nanoseconds as recently demonstrated for isobutane diffusion in silicalite.[32] The timescale limitation of the QENS instrument must be taken into account when making direct comparisons between the MD simulations and QENS measurements in this study. The limited experimental sampling of residence times would give differing diffusion coefficients from the MD simulations (able to sample all residence times), and crucially a differing trend in diffusion coefficients with temperature which dictates the measured activation energy. We propose that this resolution limitation may make a contribution to the difference in activation energy observed between theory and experiment for the Cu-CHA system.

The consistent observation of jump diffusion at all temperatures experimentally for both the CHA and Cu-CHA system with similar length and residence times (and overall self-diffusivities within experimental error of each other) suggests that on this time and length scale, the copper presence is not significantly affecting ammonia diffusion, while observation of the MD simulations show that some ammonia molecules in Cu-CHA coordinate to the Cu^{2+} ion in the centre of the chabazite cage, allowing other ammonia molecules to diffuse. As mentioned, and suggested by the trajectory plot in figure 8, the positioning of this coordinated cluster in the centre of the chabazite cage in the MD simulation suggests that the jump diffusion we observe in the QENS experiments may be transport through the 8-ring windows linking the chabazite cages (consistent with the 3 Å jump distance observed), as this would take place independently of copper presence, with the coordinating NH_3 molecules shielding the interaction of Cu^{2+} with the diffusing NH_3.

The observation that a fraction of ammonia molecules become immobilised while another fraction is free to diffuse has been observed previously in silicalite by Jobic and co-workers,[24] with immobilisation due to strong interaction with silanol groups up to temperatures of 480 K in silicalite. As in this work, an immobile ammonia molecule was defined as remaining in position for timescale on the limit of the QENS experiment, the

movement of which was resolved by the much larger timescale of PFG-NMR experiments. Ammonia temperature programmed desorption experiments performed have confirmed that complete ammonia desorption occurs at temperatures greater than 700 K for the samples studied, illustrating further the strength of NH_3 binding.[48]

Previous QENS studies have shown that the counterion does influence the diffusion of an adosrbed molecule. For example, the presence of a counter ion in Na-ZSM5 was found to lower the diffusion coefficient of a long chain alkane by a factor of ~5 compared to silicalite.[33, 34] In our study we have focused on a much smaller molecule, for which our combination of QENS and MD has shown that even in small pore zeolites the presence of a counter ion does not necessarily block motion such as intercage diffusion, as the coordination of molecules around the counterion plays a shielding role, allowing other molecules to diffuse unaffected.

4. Summary and Conclusions

The effect of counterion presence on ammonia diffusion in NH_3-SCR catalyst, small pore zeolite chabazite was studied using QENS experiments and MD simulations. QENS studies observed a jump diffusion mechanism and suggest that on the timescales observed by the experiment, the presence of a copper cation does not significantly influence the apparent diffusion coefficient of ammonia. Previous QENS studies of ammonia diffusion in silicalite have shown the presence of both mobile and immobile molecules due to interaction with silanol groups in the silicalite framework. Our MD simulations suggest a similar effect in Cu-CHA, with a fraction of NH_3 molecules coordinating strongly with the Cu^{2+} counterion in the centre of the chabazite cage, allowing diffusion through the 8-ring windows of the chabazite cage (consistent with the jump distances observed by QENS) to go ahead unimpeded. The QENS experiments and MD simulations give good agreement in terms of self-diffusion coefficient absolute values for both the H-CHA and Cu-CHA system, and the activation energy of diffusion for the CHA system; however there is a significant difference in the activation energy of diffusion between methods for the Cu-CHA system. This difference may be attributed to the differing range of residence times sampled between theory and experiment for this system and there may be a contributing factor due to the use of a

generic force field containing inherent approximations in the representation guest-host interactions. The combination of techniques has highlighted the complexity of sorbate mobility in automotive catalysts, and the relationship between counterion presence on overall mobility of sorbates in small more zeolites.

Acknowledgements

The authors acknowledge the ISIS Pulsed Neutron and Muon Source for access to beamline facilities (Experiment RB:1520464), and for funding and sponsorship of AJOM, the assistance of Dr Stewart Parker during the experimental stage and following discussions. We acknowledge the Engineering and Physical Sciences Research Council (EPSRC): grant no. EP/G036675/1 for financial support under their Centres for Doctoral Training scheme and the Science and Technologies Facilities Council. The UK Catalysis Hub is kindly thanked for resources and support provided *via* our membership of the UK Catalysis Hub Consortium and funded by EPSRC (grants EP/K014706/1, EP/K014668/1, EP/K014854/1EP/K014714/1 and EP/M013219/1).

References

1. R. M. Heck, R. J. Farrauto and S. T. Gulati, *Catalytic air pollution control: commercial technology*, John Wiley & Sons, 2009.
2. S. Brandenberger, O. Kröcher, A. Tissler and R. Althoff, *Catalysis Reviews*, 2008, **50**, 492-531.
3. A. M. Beale, F. Gao, I. Lezcano-Gonzalez, C. H. Peden and J. Szanyi, *Chemical Society Reviews*, 2015, **44**, 7371-7405.
4. B. Coq, M. Mauvezin, G. Delahay, J.-B. Butet and S. Kieger, *Applied Catalysis B: Environmental*, 2000, **27**, 193-198.
5. B. Coq, M. Mauvezin, G. Delahay and S. Kieger, *Journal of Catalysis*, 2000, **195**, 298-303.
6. A. M. Frey, S. Mert, J. Due-Hansen, R. Fehrmann and C. H. Christensen, *Catalysis letters*, 2009, **130**, 1-8.
7. C. H. Peden, J. H. Kwak, S. D. Burton, R. G. Tonkyn, D. H. Kim, J.-H. Lee, H.-W. Jen, G. Cavataio, Y. Cheng and C. K. Lambert, *Catalysis today*, 2012, **184**, 245-251.
8. L. Xie, F. Liu, L. Ren, X. Shi, F.-S. Xiao and H. He, *Environmental science & technology*, 2013, **48**, 566-572.
9. I. Nova and E. Tronconi, *Urea-SCR technology for deNOx after treatment of Diesel exhausts*, Springer, 2014.
10. J. Andersen, E. Bailie, L. Casci, H. Chen, M. Fedeyko, S. Foo and R. Rajaram, *International Publication Date*, 2008, **6**.

11. I. Bull, W.-M. Xue, P. Burk, R. S. Boorse, W. M. Jaglowski, G. S. Koermer, A. Moini, J. A. Patchett, J. C. Dettling and M. T. Caudle, *Journal*, 2009.
12. P. J. Andersen, H.-Y. Chen, J. M. Fedeyko and E. Weigert, *Journal*, 2011.
13. I. Bull, A. Moini, G. S. Koermer, J. A. Patchett, W. M. Jaglowski and S. Roth, *Journal*, 2010.
14. J. H. Kwak, R. G. Tonkyn, D. H. Kim, J. Szanyi and C. H. Peden, *Journal of Catalysis*, 2010, **275**, 187-190.
15. T. Nijhuis, L. Van den Broeke, M. Linders, J. Van de Graaf, F. Kapteijn, M. Makkee and J. Moulijn, *Chemical Engineering Science*, 1999, **54**, 4423-4436.
16. J. Kärger, D. M. Ruthven and D. N. Theodorou, *Diffusion in nanoporous materials*, John Wiley & Sons, 2012.
17. F. Gao, J. H. Kwak, J. Szanyi and C. H. Peden, *Topics in Catalysis*, 2013, **56**, 1441-1459.
18. F. Gao, E. D. Walter, E. M. Karp, J. Luo, R. G. Tonkyn, J. H. Kwak, J. Szanyi and C. H. Peden, *Journal of Catalysis*, 2013, **300**, 20-29.
19. J. H. Kwak, D. Tran, S. D. Burton, J. Szanyi, J. H. Lee and C. H. Peden, *Journal of Catalysis*, 2012, **287**, 203-209.
20. D. W. Fickel and R. F. Lobo, *The Journal of Physical Chemistry C*, 2009, **114**, 1633-1640.
21. S. T. Korhonen, D. W. Fickel, R. F. Lobo, B. M. Weckhuysen and A. M. Beale, *Chemical Communications*, 2011, **47**, 800-802.
22. U. Deka, A. l. Juhin, E. A. Eilertsen, H. Emerich, M. A. Green, S. T. Korhonen, B. M. Weckhuysen and A. M. Beale, *The Journal of Physical Chemistry C*, 2012, **116**, 4809-4818.
23. A. Möller, A. P. Guimaraes, R. Gläser and R. Staudt, *Microporous and Mesoporous Materials*, 2009, **125**, 23-29.
24. H. Jobic, H. Ernst, W. Heink, J. Kärger, A. Tuel and M. Bée, *Microporous and mesoporous materials*, 1998, **26**, 67-75.
25. C. Forste, A. Germanus, J. Karger, G. Mobius, M. Bulow, S. Zdanov and N. Feoktistova, *ISOTOPENPRAXIS*, 1989, **25**, 48-52.
26. O. Geier, S. Vasenkov, D. Freude and J. Kärger, *Journal of Catalysis*, 2003, **213**, 321-323.
27. S. Kouva, J. Kanervo, F. Schüßler, R. Olindo, J. A. Lercher and O. Krause, *Chemical Engineering Science*, 2013, **89**, 40-48.
28. L. Forni, F. P. Vatti and E. Ortoleva, *Microporous Materials*, 1995, **3**, 367-375.
29. H. Jobic and D. N. Theodorou, *Microporous and mesoporous materials*, 2007, **102**, 21-50.
30. A. J. O'Malley and C. R. A. Catlow, *Physical Chemistry Chemical Physics*, 2013, **15**, 19024-19030.
31. A. J. O'Malley and C. R. A. Catlow, *Physical Chemistry Chemical Physics*, 2015, **17**, 1943-1948.
32. A. J. O'Malley, C. R. A. Catlow, M. Monkenbusch and H. Jobic, *The Journal of Physical Chemistry C*, 2015, **119**, 26999-27006.
33. H. Jobic and D. N. Theodorou, *The Journal of Physical Chemistry B*, 2006, **110**, 1964-1967.
34. H. Jobic, *Journal of Molecular Catalysis A: Chemical*, 2000, **158**, 135-142.
35. M. T. Telling and K. H. Andersen, *Physical Chemistry Chemical Physics*, 2005, **7**, 1255-1261.
36. O. Arnold, J.-C. Bilheux, J. Borreguero, A. Buts, S. I. Campbell, L. Chapon, M. Doucet, N. Draper, R. F. Leal and M. Gigg, *Nuclear Instruments and Methods in Physics Research Section A: Accelerators, Spectrometers, Detectors and Associated Equipment*, 2014, **764**, 156-166.
37. R. T. Azuah, L. R. Kneller, Y. Qiu, P. L. Tregenna-Piggott, C. M. Brown, J. R. Copley and R. M. Dimeo, *Journal of Research of the National Institute of Standards and Technology*, 2009, **114**, 341.
38. B. Materials Studio 8.0, Dassault Systèmes, 5005 Wateridge Vista Drive, San Diego, CA 92121 USA *Journal*.
39. http://www.iza-structure.org/databases/.
40. B. M. K. Alvardo-Swaisgood A.E. , Hay P.J. , Redondo A., *J. Phys. Chem.*, 1991, 10031.
41. M. Davidová, D. Nachtigallová, P. Nachtigall and J. Sauer, *The Journal of Physical Chemistry B*, 2004, **108**, 13674-13682.

42. H. Sun, *The Journal of Physical Chemistry B*, 1998, **102**, 7338-7364.
43. M. U. Arı, M. G. k. Ahunbay, M. Yurtsever and A. Erdem-Senatalar, *The Journal of Physical Chemistry B*, 2009, **113**, 8073-8079.
44. C. Chudley and R. Elliott, *Proceedings of the Physical Society*, 1961, **77**, 353.
45. A. R. Teixeira, X. Qi, C.-C. Chang, W. Fan, W. C. Conner and P. J. Dauenhauer, *The Journal of Physical Chemistry C*, 2014, **118**, 22166-22180.
46. M. Diraison, G. Martyna and M. Tuckerman, *The Journal of chemical physics*, 1999, **111**, 1096-1103.
47. E. S. Shpiro, W. Grünert, R. W. Joyner and G. N. Baeva, *Catalysis letters*, 1994, **24**, 159-169.
48. P. S. Metkar, V. Balakotaiah and M. P. Harold, *Chemical engineering science*, 2011, **66**, 5192-5203.